Precision crystal calorimeters in high-energy physics: past, present, and future

Ren-Yuan Zhu

Ren-Yuan Zhu, "Precision crystal calorimeters in high-energy physics: past, present, and future," Proc. SPIE 7079, Hard X-Ray, Gamma-Ray, and Neutron Detector Physics X, 70790W (4 September 2008); doi: 10.1117/12.796834

SPIE.

Event: Optical Engineering + Applications, 2008, San Diego, California, United States

Precision Crystal Calorimeters in High Energy Physics: Past, Present and Future

Ren-Yuan Zhu[a]

[a]California Institute of Technology, Pasadena, CA 91125, USA

ABSTRACT

Precision crystal calorimeter traditionally plays an important role in experimental high energy physics. In the last two decades, it faces a challenge to maintain its precision in a hostile radiation environment. This paper reviews the performance of crystal calorimeters constructed for high energy physics experiment and the progress achieved in understanding crystal's radiation damage and in developing high quality scintillating crystals. Future crystal calorimeters, such as a LSO and LYSO calorimeter and homogeneous hadronic calorimeter, being considered for experimental particle physics is also discussed.

Keywords: Crystal, calorimeter, scintillator

1. INTRODUCTION

Total absorption shower counters made of inorganic crystal scintillators have been known for decades for their superb energy resolution and detection efficiency.[1] In high energy and nuclear physics, large arrays of scintillating crystals have been assembled for precision measurement of photons and electrons. The physics discovery potential of crystal calorimeter was early demonstrated by the Crystal Ball experiment through its study of radiative transitions and decays of the Charmonium family.[2] Figure 1 (Left) shows nearly all the principal radiative transition lines of the Charmonium system simultaneously measured by the NaI(Tl) crystal calorimeter. The

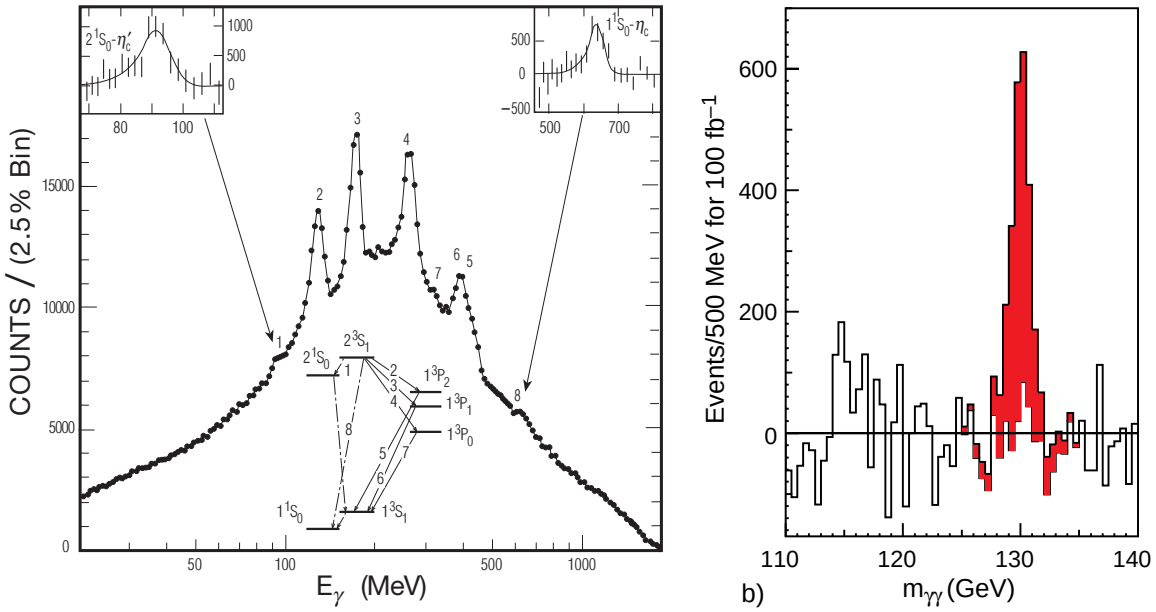

Figure 1. Left: An inclusive photon spectrum measured at the ψ' by the NaI(Tl) crystal calorimeter of the Crystal Ball experiment at SLAC.[2] Right: The expected background subtracted Higgs mass peak reconstructed from its two photon decays measured by the CMS $PbWO_4$ crystal calorimeter.[3]

Corresponding author: Ren-yuan Zhu, E-mail: zhu@hep.caltech.edu, Telephone: 1 626 395 6661

Hard X-Ray, Gamma-Ray, and Neutron Detector Physics X, edited by Arnold Burger, Larry A. Franks, Ralph B. James,
Proc. of SPIE Vol. 7079, 70790W, (2008) · 0277-786X/08/$18 · doi: 10.1117/12.796834

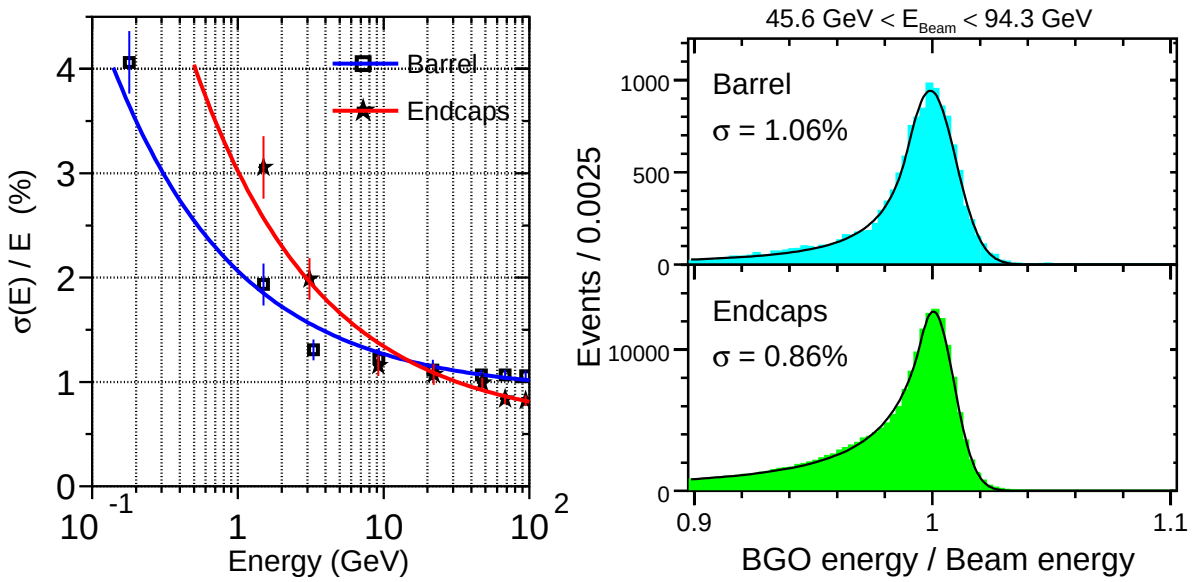

Figure 2. Left: The energy resolution of the L3 BGO calorimeter as a function of electron energy measured in the CERN test beam. Right: The energy resolution of Bhabha electrons observed by the L3 BGO calorimeter *in situ* at LEP by using the RFQ calibration.

designed goal of the CMS lead tungstate ($PbWO_4$) crystal calorimeter[3] is to maximize its physics discovery potential in searching for narrow resonances in photon and electron final states at LHC. Figure 1 (Right) shows the expected background subtracted Higgs peak reconstructed with its two decay photons by the CMS $PbWO_4$ calorimeter. The ability of the Higgs discovery via this decay channel is directly related to the energy resolution of the calorimeter.

Crystal calorimeters have been constructed, and their use has been a key factor in the successful physics programs of many experiments. With proper calibration and monitoring, crystal calorimeters usually achieve their designed resolution *in situ*.[4] Figure 2 (Left) shows energy resolution as a function of the electron energy obtained with the L3 BGO calorimeter in the CERN test beam, which is in a good agreement with the resolution of Bhabha electrons reconstructed *in situ* at LEP, as shown in Figure 2 (Right). To achieve this resolution a radio frequency quadrupole accelerator based calibration technique was used,[5]

Table 1. Crystal Calorimeter in High Energy Physics: Past and Present

Experiment	C. Ball	L3	CLEO II	KTeV	*BaBar*	BELLE	CMS
Accelerator	SPEAR	LEP	CESR	Tevatron	PEP II	KEK	LHC
Date	75–85	80–00	80–00	90–10	94–10	94–10	95–20
Crystal Type	NaI(Tl)	BGO	CsI(Tl)	CsI	CsI(Tl)	CsI(Tl)	$PbWO_4$
B-Field (Tesla)	-	0.5	1.5	-	1.5	1.0	4.0
Inner Radius (m)	0.254	0.55	1.0	-	1.0	1.25	1.29
Number of Crystals	672	11,400	7,800	3,300	6,580	8,800	76,000
Crystal Depth (X_0)	16	22	16	27	16 to 17.5	16.2	25
Crystal Volume (m^3)	1	1.5	7	2	5.9	9.5	11
L. Yield (p.e./MeV)	350	1,400	5,000	40	5,000	5,000	2
Photosensor	PMT	Si PD	Si PD	PMT	Si PD	Si PD	APD†
Photosensor Gain	Large	1	1	4,000	1	1	50
Noise/Chan. (MeV)	0.05	0.8	0.5	Small	0.15	0.2	30
Dynamic Range	10^4	10^5	10^4	10^4	10^4	10^4	10^5

† Avalanche photo-diode.

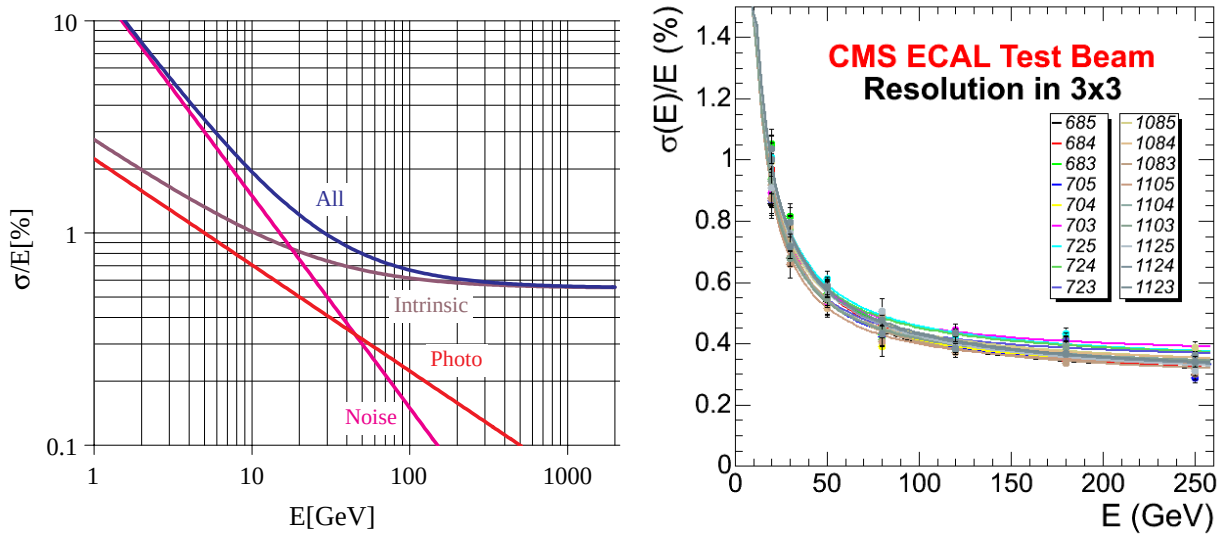

Figure 3. Left: The designed energy resolution of the CMS $PbWO_4$ calorimeter and corresponding contributions is shown as a function of energy .[3] Right: The energy resolution of two groups of 9 $PbWO_4$ crystals is shown as function of electron energy obtained in the CMS ECAL beam test.[6]

Table 1 summarizes parameters of past and present crystal calorimeters in high energy physics. One notes that each of these calorimeters requires several cubic meters of high quality crystals. The most ambitious crystal calorimeter in Table 1 is presumably the CMS calorimeter which uses 11 m^3 $PbWO_4$ crystals. Its designed energy resolution[3] is

$$\sigma_E/E = \mathbf{2.7}\%/\sqrt{E} \oplus \mathbf{0.55}\% \oplus 0.16/E \quad (1)$$

for the barrel, and

$$\sigma_E/E = \mathbf{5.7}\%/\sqrt{E} \oplus \mathbf{0.55}\% \oplus 0.77/E \quad (2)$$

for the endcaps.

Figure 3 (Left) shows the designed energy resolution as a function of energy for the CMS $PbWO_4$ calorimeter. It can be decomposed to three contributions from photo-electron statistics (stochastic), intrinsic shower leakage (stochastic and constant) and readout noise (noise). Figure 3 (Right) shows the energy resolution as a function of electron energy measured in the CERN test beam for two groups of 3×3 crystals, independent of their impact position on the crystal front face.[6] The measured resolution in the low and middle energy region agrees well with the designed resolution. At the high energy region, the measured energy resolution is better than the design values since there is no calibration uncertainty in the test beam data.

Because of the increased center of mass energy and luminosity, however, crystal calorimeters faced a new challenge in the last decade: radiation damage. To preserve the calorimeter precision offered by crystals in a severe radiation environment crystal quality control is a crucial issue. Section 2 of this paper discusses optical and scintillation properties of heavy crystal scintillators commonly used in particle physics experiment. The progresses achieved over the last two decades in understanding crystal's radiation damage and in developing high quality crystals are described in sections 3 and 4 respectively. Finally, section 5 discusses the performance of future crystal calorimeter made by LSO and LYSO crystals and a crystal hadronic calorimeter concept for high energy physics applications.

2. PROPERTIES OF CRYSTAL SCINTILLATORS

Table 2[7] lists basic properties heavy crystal scintillators: NaI(Tl), CsI(Tl), undoped CsI, BaF_2, CeF_3, bismuth gemanade ($Bi_4Ge_3O_{12}$ or BGO), lead tungstate ($PbWO_4$ or PWO) and Ce-doped lutetium oxyorthosilicate ($Lu_2(SiO_4)O$ or LSO(Ce)).[8] All, except CeF_3, have either been used in, or actively pursued for, high energy and nuclear physics experiments. LSO(Ce) and cerium doped lutetium yttrium oxyorthosilicate ($Lu_{2(1-x)}Y_{2x}SiO_5$:Ce, LYSO)[9] are widely used in the medical industry. Mass production capabilities exist for all these crystals.

Table 2. Properties of Heavy Crystal Scintillators with Mass Production Capability

Crystal	NaI(Tl)	CsI(Tl)	CsI	BaF_2	CeF_3	BGO	$PbWO_4$	LSO(Ce)
Density (g/cm^3)	3.67	4.51	4.51	4.89	6.16	7.13	8.3	7.40
Melting Point (°C)	651	621	621	1280	1460	1050	1123	2050
Radiation Length (cm)	2.59	1.86	1.86	2.03	1.70	1.12	0.89	1.14
Molière Radius (cm)	4.13	3.57	3.57	3.10	2.41	2.23	2.00	2.07
Interaction Length (cm)	42.9	39.3	39.3	30.7	23.2	22.7	20.7	20.9
Refractive Index[a]	1.85	1.79	1.95	1.50	1.62	2.15	2.20	1.82
Hygroscopicity	Yes	Slight	Slight	No	No	No	No	No
Luminescence[b] (nm)	410	560	420	300	340	480	425	420
(at Peak)			310	220	300		420	
Decay Time[b] (ns)	245	1220	30	650	30	300	30	40
			6	0.9			10	
Light Yield[b,c]	100	165	3.6	36	7.3	21	0.30	85
			1.1	4.1			0.077	
d(LY)/dT[b,d] (%/°C)	-0.2	0.4	-1.4	-1.9	∼0	-0.9	-2.5	-0.2
				0.1				
Experiment	Crystal Ball	CLEO *BaBar* BELLE BES III	KTeV	TAPS	-	L3 BELLE	CMS ALICE PrimEx Panda	SuperB

a At the wavelength of the emission maximum.
b Top line: slow component, bottom line: fast component.
c Relative light yield of samples of 1.5 X_0 and with the PMT quantum efficiency taken out.
d At room temperature.

Figure 4 is a photo showing twelve crystal samples. In addition to samples listed in Table 2 CsI(Na), LYSO and two recently discovered cerium doped lanthanum tri-halides, $LaCl_3$ and $LaBr_3$,[10] are also shown in this

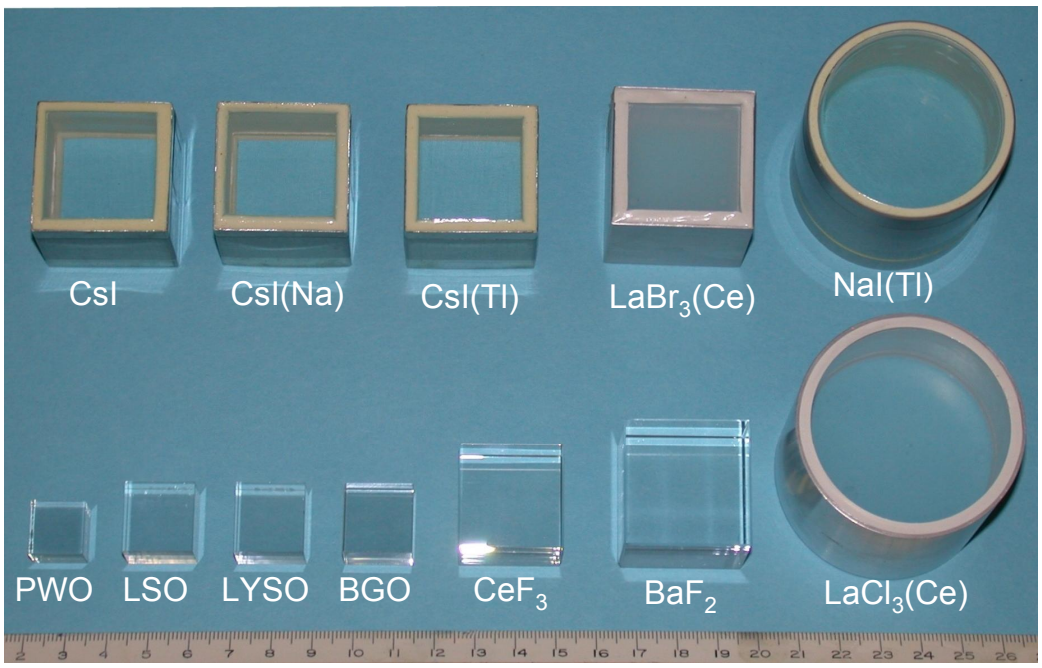

Figure 4. A photo shows twelve crystal scintillators with dimension of 1.5 X_0.

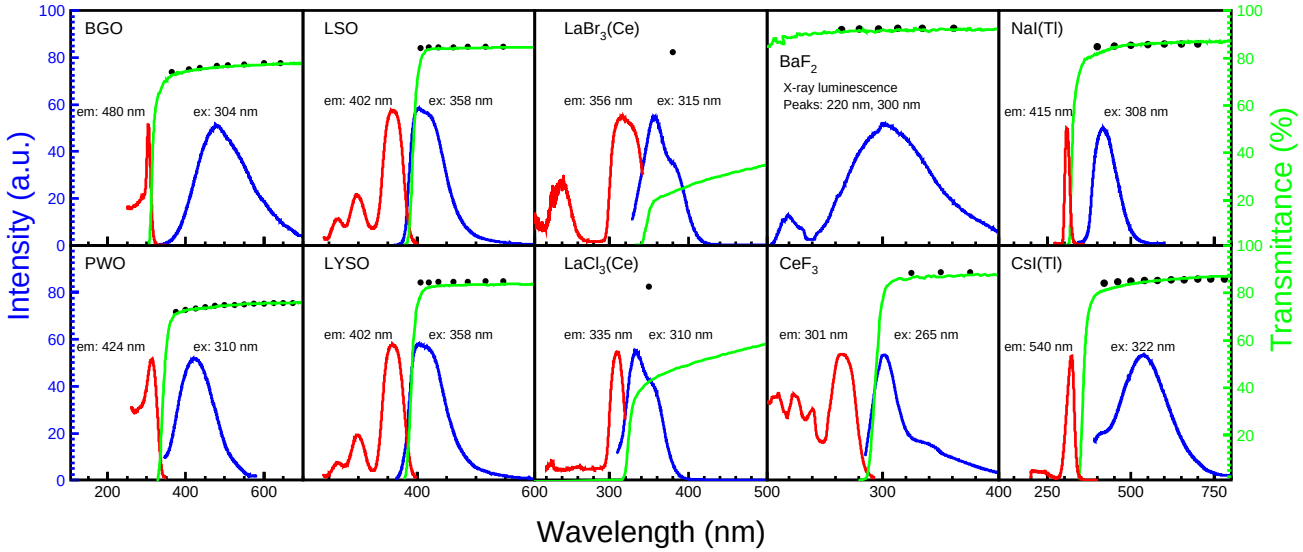

Figure 5. The excitation (red) and emission (blue) spectra (left scale) and the transmittance (green) spectra (right scale) are shown as a function of wavelength for ten crystal scintillators with solid black dots showing the theoretical limit of transmittance.

photo although they are not yet in mass production stage. Samples are arranged in an order of their density, or radiation length. All non-hygroscopic samples are wrapped with white Tyvek paper as reflector. Hygroscopic NaI, CsI, $LaBr_3$ and $LaCl_3$ are sealed in package with two ends made of quartz windows of 3 or 5 mm thick to avoid surface degradation. To minimize uncertainties in light output measurement caused by the sample size dependence all samples have a cubic shape of $1.5 \times 1.5 \times 1.5$ X_0^3, except NaI(Tl) and $LaCl_3$ which are a cylinder with a length of 1.5 X_0 and areas at two ends equaling to 1.5×1.5 X_0^2 to match the 2 inch diameter of the PMT cathode.

Figure 5 shows a comparison of the transmittance, emission and excitation (dashed lines) spectra as a function of wavelength for ten samples. The solid black dots in these plots are the theoretical limit of the transmittance, which was calculated by using corresponding refractive index as a function of wavelength taking into account multiple bounces between the two parallel end surfaces and assuming no internal absorption.[11] Most samples, except $LaBr_3$ and $LaCl_3$, have their transmittance approaching the theoretical limits, indicating negligible internal absorption. The poor transmittance measured for $LaBr_3$ and $LaCl_3$ samples is probably due to scattering

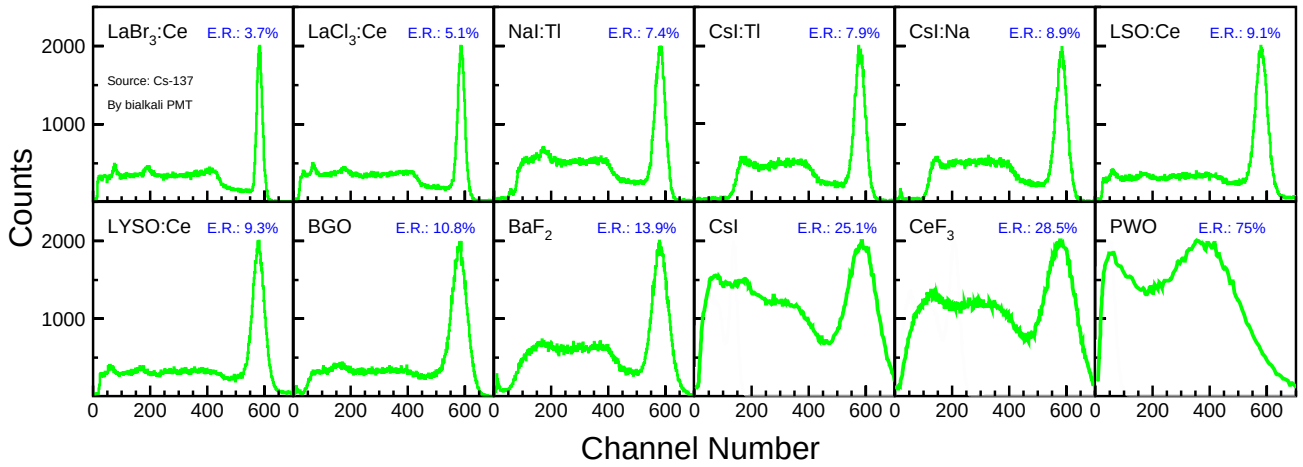

Figure 6. ^{137}Cs γ-ray pulse hight spectra measured by a Hamamatsu R1306 PMT for twelve crystal samples with numerical values of the FWHM resolution (E.R.) also shown in the figure.

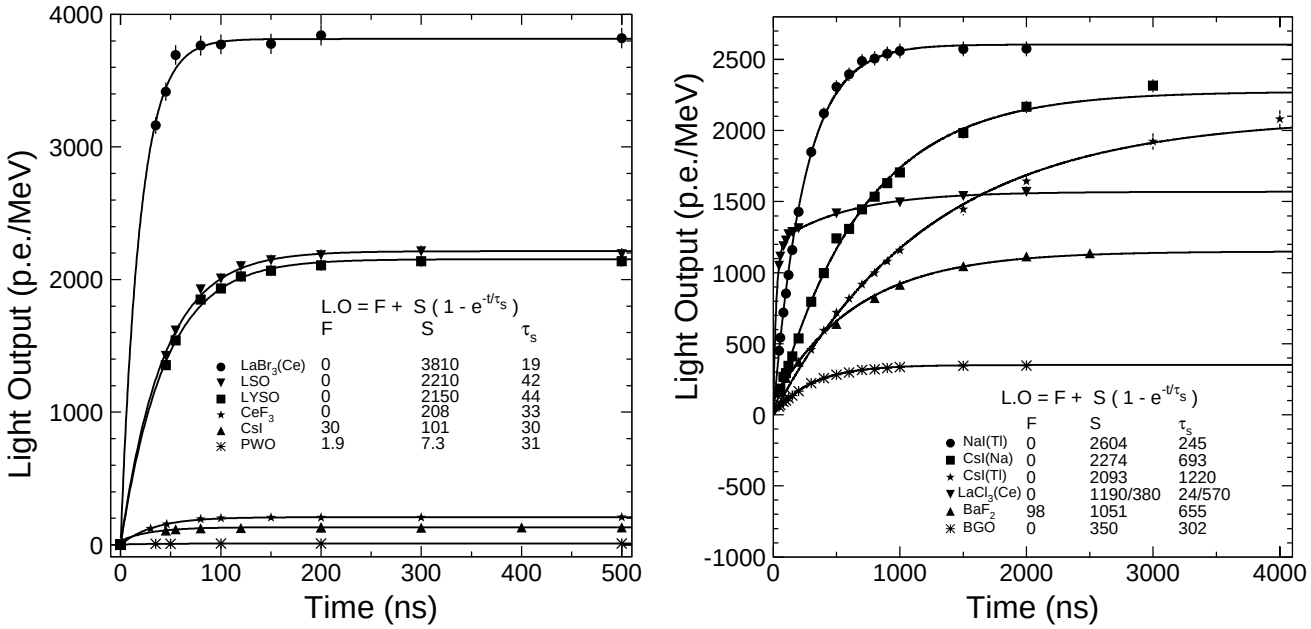

Figure 7. Light output measured by using a XP2254b PMT is shown as a function of integration time for fast (Left) and slow (Right) crystal scintillators.

centers inside these samples.

It is interesting to note that the BaF_2, BGO, NaI(Tl), CsI(Tl) and $PbWO_4$ crystals have their emission

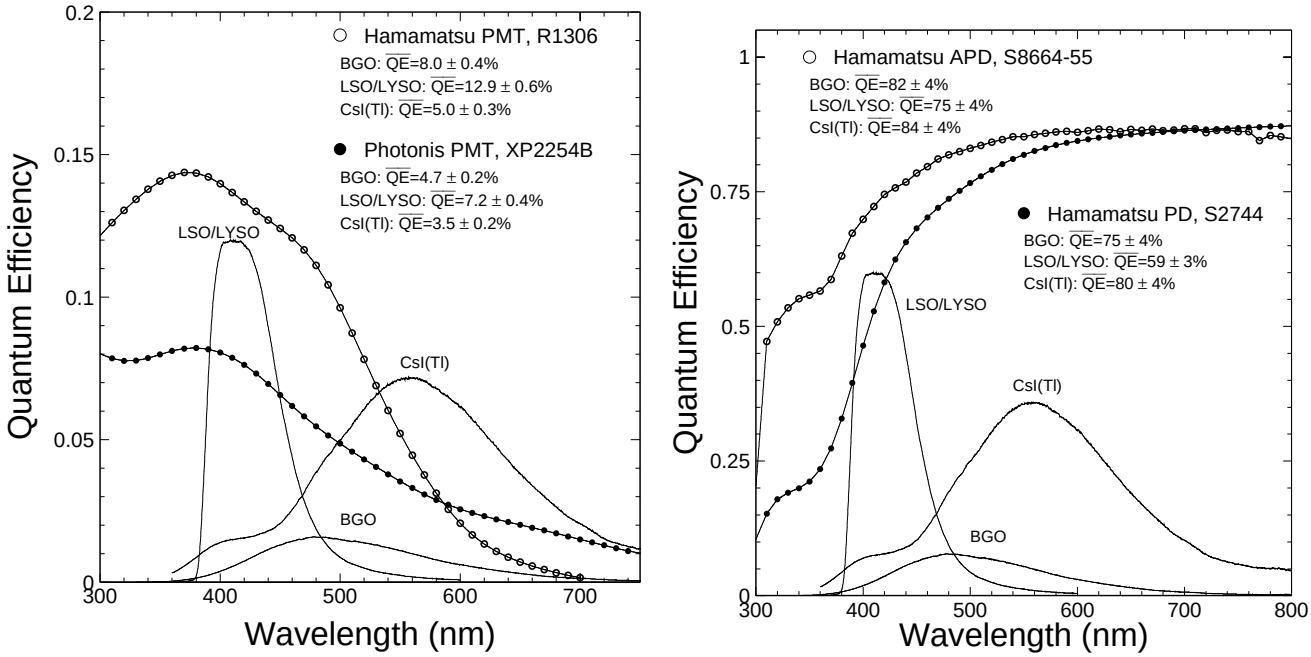

Figure 8. Left: Quantum efficiencies of a Hamamatsu 1306 PMT with bi-alkali cathode (open circles) and a Photonis 2254B PMT with multi-alkali cathode (solid dots) are shown as a function of wavelength together with the emission spectra of the LSO/LYSO, BGO and CsI(Tl) samples, where the area under the emission curves is proportional to their corresponding absolute light output. Right: The same for a Hamamatsu S8664 Si APD (open circles) and a Hamamatsu S2744 Si PIN diode (solid dots).

Table 3. Emission Weighted Quantum Efficiencies (%)

Emission	LSO/LYSO	BGO	CsI(Tl)
Hamamatsu R1306 PMT	12.9±0.6	8.0±0.4	5.0±0.3
Hamamatsu R2059 PMT	13.6±0.7	8.0±0.4	5.0±0.3
Photonis XP2254b	7.2±0.4	4.7±0.2	3.5±0.2
Hamamatsu S2744 PD	59±4	75±4	80±4
Hamamatsu S8664 APD	75±4	82±4	84±4

spectra well within the transparent region showing no obvious self-absorption. The UV absorption edge in the transmittance spectra of the LSO, LYSO, CeF_3, $LaBr_3$ and $LaCl_3$ crystals, however, cuts into the emission spectra and thus affects crystal's light output. This self-absorption effect is more seriously in long crystal samples used in high energy and nuclear physics experiment as extensively discussed for LSO and LYSO crystals.[12]

Figure 6 shows pulse hight spectra measured by a Hamamatsu R1306 PMT with bi-alkali cathode for twelve crystal samples with a ^{137}Cs γ-ray source. Also shown in these figures are the corresponding FWHM energy resolution (E.R.). A better than 2% resolution is required to identify low energy γ-rays from isotopes in homeland security applications. It is clear that only the $LaBr_3$ sample approaches this requirement. All other crystals do not provide sufficient energy resolution at low energies.

Figure 7 shows light output in photoelectrons per MeV energy deposition as a function of the integration time, measured by using a Photonis XP2254b PMT with multi-alkali photo cathode, for six fast crystal scintillators (Left): $LaBr_3$, LSO, LYSO, CeF_3, undoped CsI and $PbWO_4$ and six slow crystal scintillators (Right): NaI(Tl), CsI(Na), CsI(Tl), $LaCl_3$, BaF_2 and BGO. The corresponding fits to the exponentials and their numerical results are also shown in these figures. The undoped CsI, $PbWO_4$, $LaCl_3$ and BaF_2 crystals are observed to have two decay components. Despite its poor transmittance the cerium doped $LaBr_3$ is noticed by its bright fast scintillation, leading to the excellent energy resolution for the γ-ray spectroscopic applications. The LSO and LYSO samples have consistent fast decay time (~40 ns) and photo-electron yield, which is 6 and 230 times of BGO and $PbWO_4$ respectively.

Since the quantum efficiency of the PMT used for the light output measurement is a function of wavelength, it must be taken out to directly compare crystal's light output. Figure 8 shows typical quantum efficiency as a function of wavelength for a PMT with bi-alkali cathode (Hamamatsu R1306) and a PMT with multi-alkali cathode (Photonis 2254B), a Si APD (Hamamatsu S8664) and a Si PIN PD (Hamamatsu S2744). The emission spectra of LSO/LYSO, BGO and CsI(Tl) crystals are also shown in these figures. Table 3 summarized numerical

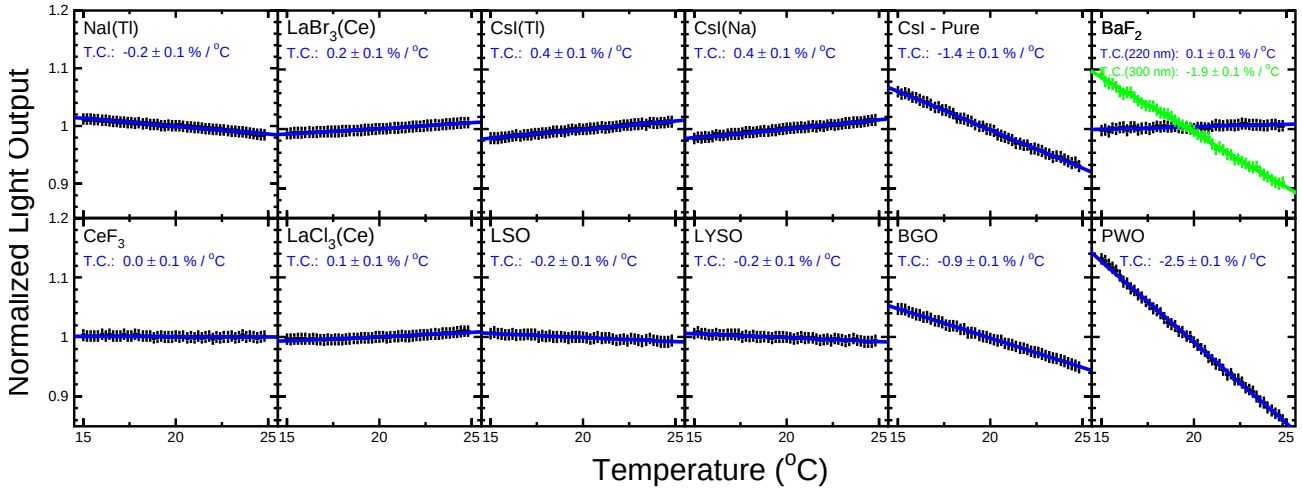

Figure 9. Light output temperature coefficient obtained from linear fits between 15°C and 25°C for twelve crystal scintillators.

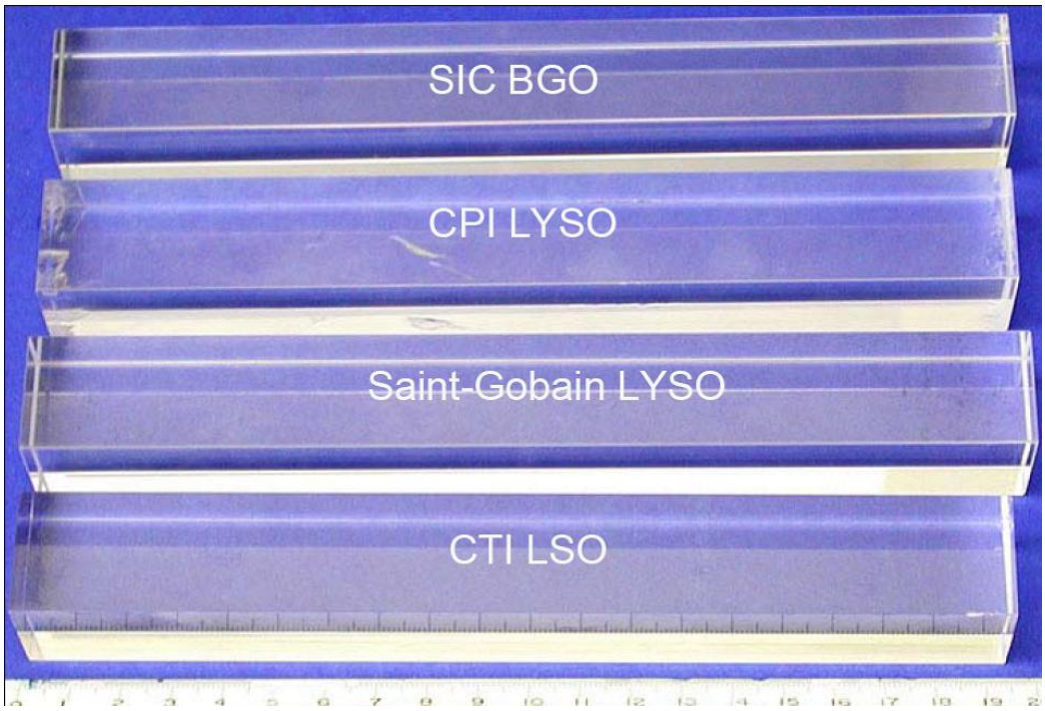

Figure 10. A photo shows four long crystal samples with dimension of $2.5 \times 2.5 \times 20$ cm^3.

result of the emission weighted average quantum efficiency for several readout devices. To facilitate a direct estimation for different readout devices the PMT quantum efficiency was taken out for the light output values listed in Table 2. With the PMT response taken out, we conclude that the light output of LSO and LYSO

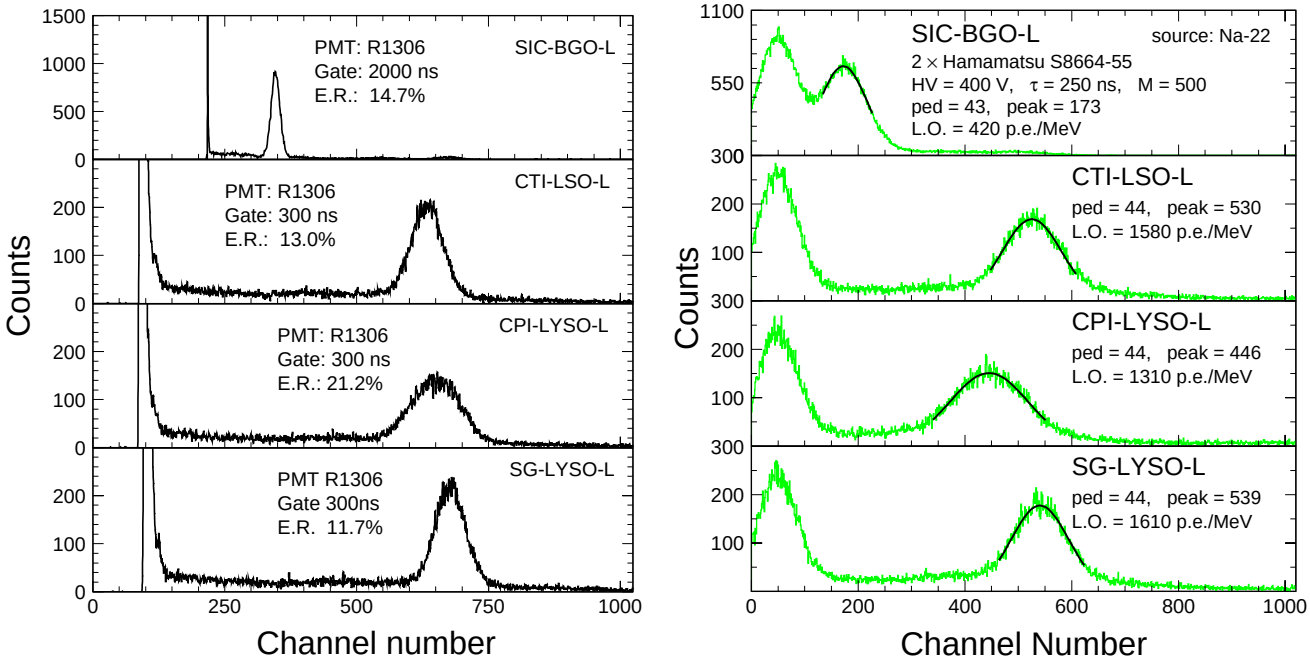

Figure 11. The spectra of 0.511 MeV γ-rays from a ^{22}Na source measured with a coincidence trigger using a Hamamatsu R1306 PMT (Left) and two Hamamatsu S8664-55 APDs (Right) for long BGO, LSO and LYSO samples of $2.5 \times 2.5 \times 20$ cm^3 size.

crystals is a factor of 4 and 200 of that of BGO and $PbWO_4$ respectively, as shown in Table 2.

Scintillation light yield from crystal scintillators may also depends on the temperature. Fig 9 shows light output variations for twelve crystal samples between 15°C and 25°C. The corresponding temperature coefficients obtained from linear fits are also listed in the figure. The numerical result of these fits is also listed in Table 2.

Large size LSO and LYSO crystals with consistent optical and scintillation properties have been developed recently for the medical industry.[12] Figure 10 shows four long crystal samples: SIC BGO, CTI LSO, CPI LYSO and Saint-Gobain LYSO of $2.5 \times 2.5 \times 20$ cm^3 size. Their availability provides a new possibility for the precision crystal calorimeters.

Figure 11[12] shows spectra of 0.51 MeV γ-rays from a ^{22}Na source observed with coincidence triggers. The readout devices used are a Hamamatsu R1306 PMT (Left) and 2 Hamamatsu S8664-55 APDs (Right). The FWHM resolution for the 0.51 MeV γ-ray with the PMT readout is about 12% to 13% for these long LSO and LYSO samples, which can be compared to 15% for the BGO sample. With APD readout, the γ-ray peaks are also visible for the long LSO and LYSO samples. The energy equivalent readout noise was less than 40 keV for these LSO and LYSO samples in our laboratory. The key issue of using LSO and LYSO crystals for precision crystal calorimeter is to maintain their longitudinal uniformity.

3. CRYSTAL RADIATION DAMAGE

All known large size crystal scintillators suffer from radiation damage.[13] There are three possible radiation damage effects in crystal scintillators. First, radiation would induce internal absorption, caused by color center formation, which would reduce the light attenuation length,[11] and thus the light output, and may also cause a degradation of the light response uniformity. Figure 12 shows the longitudinal transmittance spectra and their degradation under irradiation measured for full size CMS $PbWO_4$ (23 cm long, Left) and *BaBar* CsI(Tl) (30 cm long, Right) crystal samples respectively. The radiation induced absorption and corresponding color center formation are clearly observed in these samples.

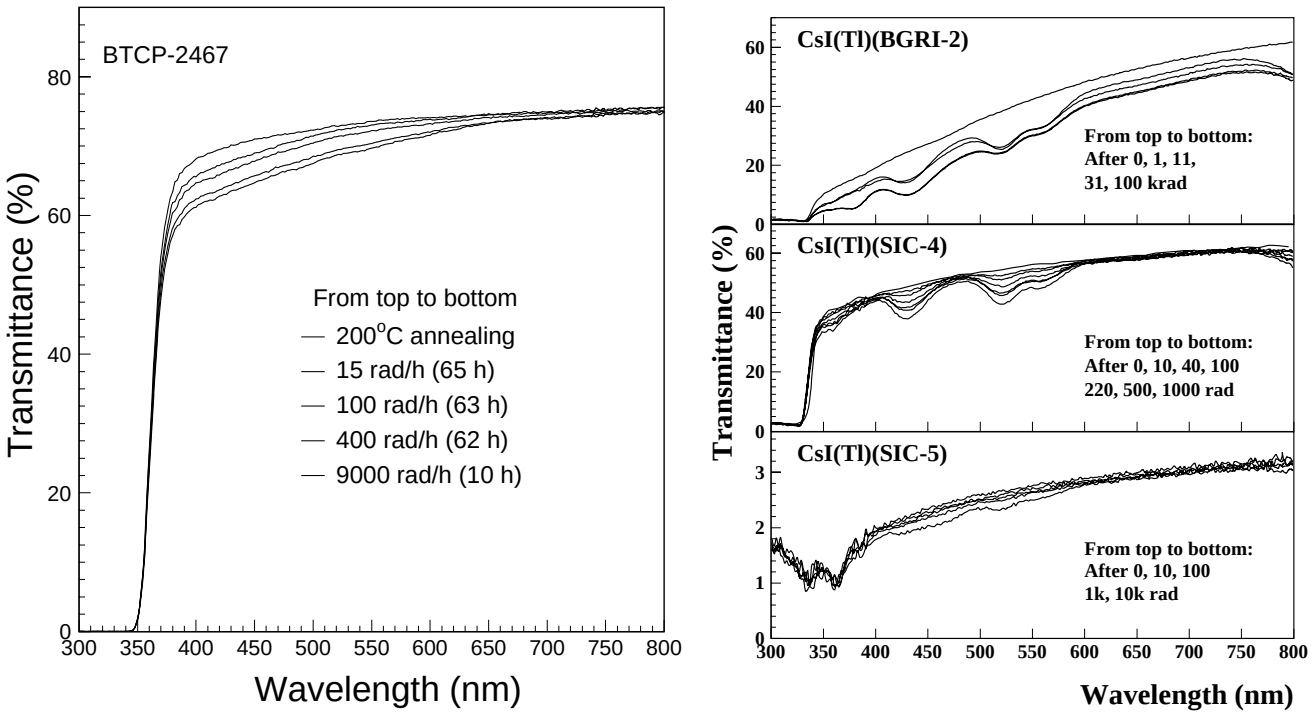

Figure 12. Longitudinal transmittance of $PbWO_4$ (Left) and CsI(Tl) (Right) samples, showing radiation induced absorption bands.

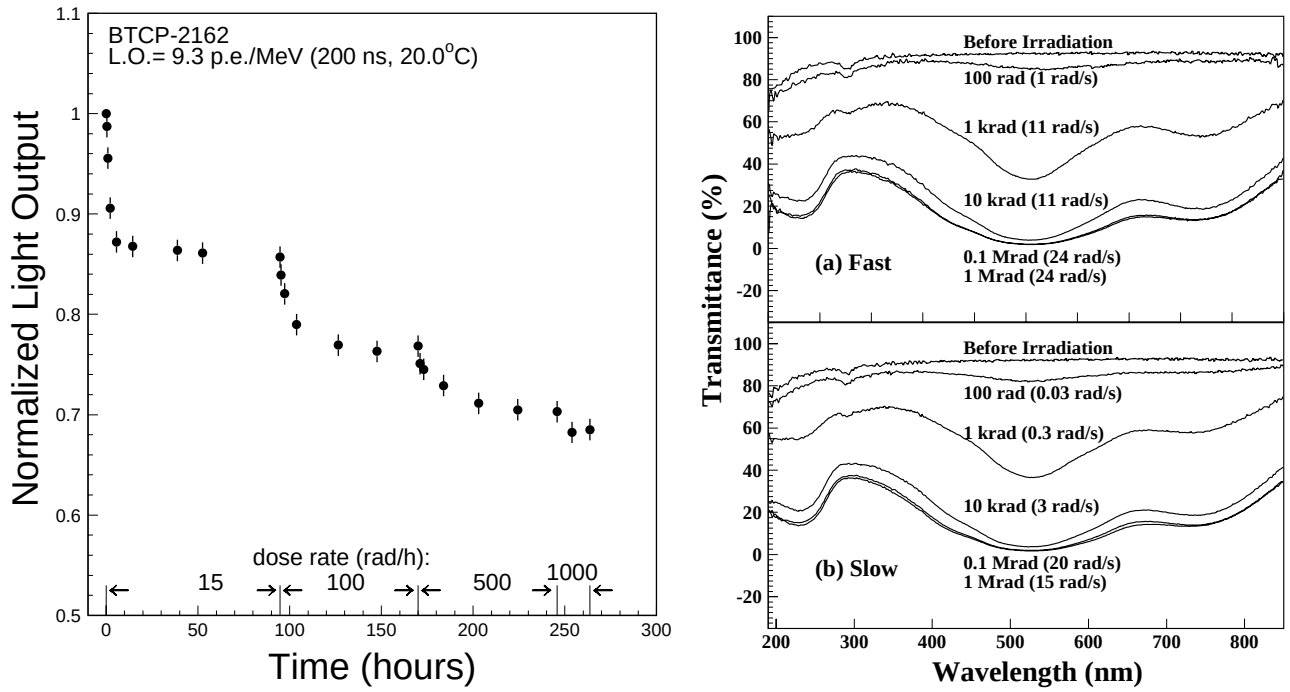

Figure 13. Left: Normalized light output is plotted as a function of time under irradiation for a CMS $PbWO_4$ sample, showing dose rate dependent radiation damage. Right: No dose rate dependence was observed for the longitudinal transmittance spectra measured for a GEM full size BaF_2 sample.

Second, radiation would induce phosphorescence (afterglow), which would cause an increase of the readout noise. Last, radiation may also reduce scintillation light yield. If so, both the light output and the light response uniformity would be degraded since the radiation dose profile *in situ* is usually not uniform.

Radiation induced absorption may also recover under application temperature through a process called color center annihilation. If so, the damage would be dose rate dependent.[13] Figures 13 (Left) shows light output normalized to that before irradiation (solid dots with error bars) as a function of time under irradiation for a full size CMS $PbWO_4$ sample. Measurements were made step by step for different dose rates: 15, 100, 500 and 1,000 rad/h, as shown in these figures. The degradation of the light output shows a clear dose rate dependence.

If no recovery or the recovery speed is very slow, however, the color center annihilation process would be less important, the color center density would not reach an equilibrium under certain dose rate rather continuous increasing until all defect traps are filled. This means no dose rate dependence. Figure 13 (Right) shows the transmittance as a function of wavelength for a GEM full size (25 cm) BaF_2 sample before and after 100, 1k, 10k, 100k and 1M rad irradiation (from top to bottom) under a fast (a) and a slow (b) dose rates. While the fast dose rate is up to a factor of thirty higher than the slow rate, the damage levels for the same integrated

Table 4. Radiation Damage in Crystal Scintillators

Item	CsI(Tl)	CsI	BaF_2	BGO	PWO	LSO/LYSO
Color Centers	Yes	Yes	Yes	Yes	Yes	Yes
phosphorescence	Yes	Yes	Yes	Yes	Yes	Yes
Scintillation Damage	No	No	No	No	No	No
Recover @RT	Slow	Slow	No	Yes	Yes	No
Dose Rate Dependence	No	No	No	Yes	Yes	No
Thermally Annealing	No	No	Yes	Yes	Yes	Yes
Optical Bleaching	No	No	Yes	Yes	Yes	Yes

dose are identical. This was expected, since no recovery at room temperature was observed for BaF_2. Crystal radiation damage may also be cured by either thermal annealing or optical bleaching.[14] Table 4 summarizes radiation damage observed in various crystal scintillators.

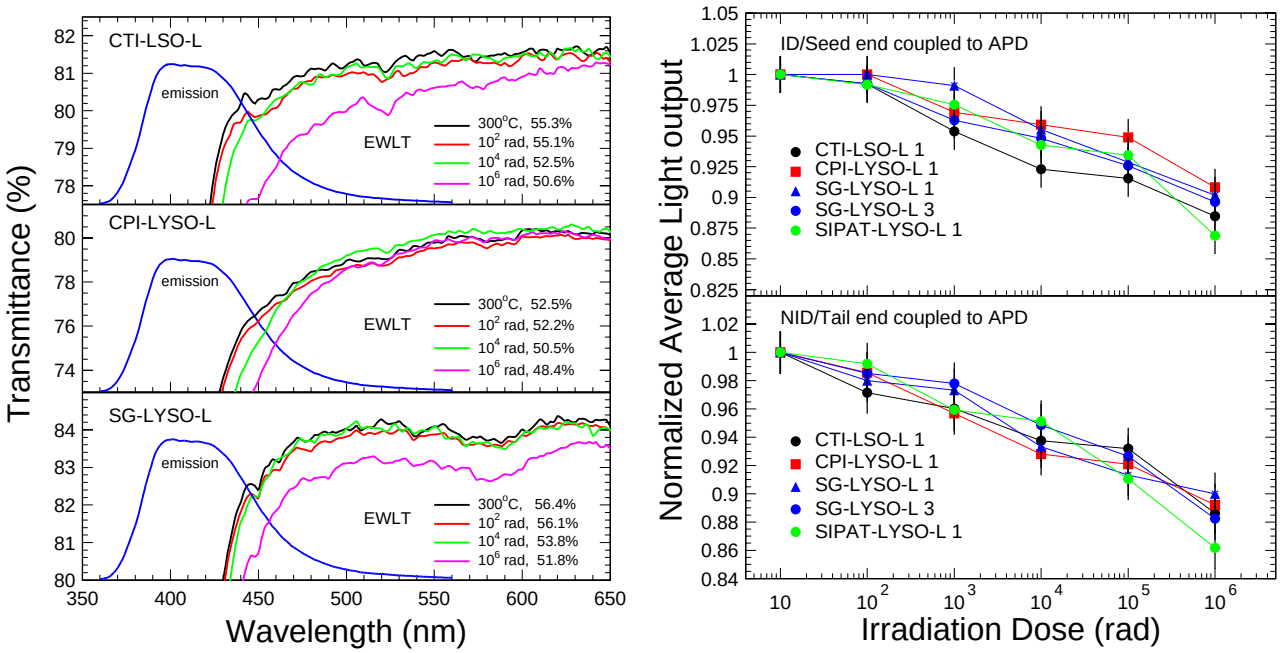

Figure 14. Left: Transmittance spectra are shown as a function of wavelength in an expanded scale together with the photo-luminescence spectra for three long LSO and LYSO samples before and after the irradiation with integrated doses of 10^2, 10^4 and 10^6 rad. Right: Normalized light output with ID (top) and NID (bottom) end coupled to the readout device of two S8664-55 APDs is shown as a function of the integration dose for five long LSO and LYSO samples.

Investigations on LSO and LYSO long samples show that the scintillation mechanism is not damaged by γ-ray irradiation, radiation damage recovers very slow under room temperature but can be completely cured by thermal annealing at 300°C for ten hours.[15] The γ-ray induced readout noise was also estimated to be about 0.2 MeV and 1 MeV equivalent respectively in a radiation environment of 15 rad/h and 500 rad/h for LYSO samples of $2.5 \times 2.5 \times 20$ cm^3 size. The overall radiation hardness of LSO/LYSO crystals is found to be much better than other crystals commonly used in high energy and nuclear physics experiment, such as BGO, CsI(Tl) and $PbWO_4$. Figure 14 (Left) shows an expanded view of the longitudinal transmittance spectra for three long samples before and after several steps of the γ-ray irradiation with integrated dose of 10^2, 10^4 and 10^6 rad. Also shown in the figure is the corresponding numerical values of the photo-luminescence weighted longitudinal transmittance ($EWLT$). Figure 14 (Right) shows the normalized average light output as a function of integrated dose for five long LSO and LYSO samples from CTI, CPI, Saint-Gobain and SIPAT. It is interesting to note that all samples show consistent radiation resistance with light output degradation at 10 to 15% level after γ-ray irradiation with an integrated dose of 1 Mrad.

4. CRYSTAL DEVELOPMENT AND QUALITY IMPROVEMENT

Commercially available mass produced crystals usually do not meet the quality required for precision crystal calorimeter. A research and development program is usually needed to systematically study the correlations between crystal's radiation hardness and its impurities and point defects. By removing harmful impurities from the raw materials and adapting an approach to effectively reduce defect related color center density in the crystal during the growth and processing, the quality of mass produced crystals may be improved. Such development has been successfully carried out for BGO,[16] BaF_2,[17] CsI(Tl)[13] and $PbWO_4$.[13,18] Two examples are given below in this section.

4.1 CsI(Tl) Development

Figure 15 (Left) shows the normalized light output as a function of integrated dose for full size ($\sim$ 30 cm) CsI(Tl) samples produced at the Shanghai Institute of Ceramics (SIC), and compared to the *BaBar* radiation hardness specification (solid line).[13] While the late samples SIC-5, 6, 7 and 8 satisfy the *BaBar* specification,

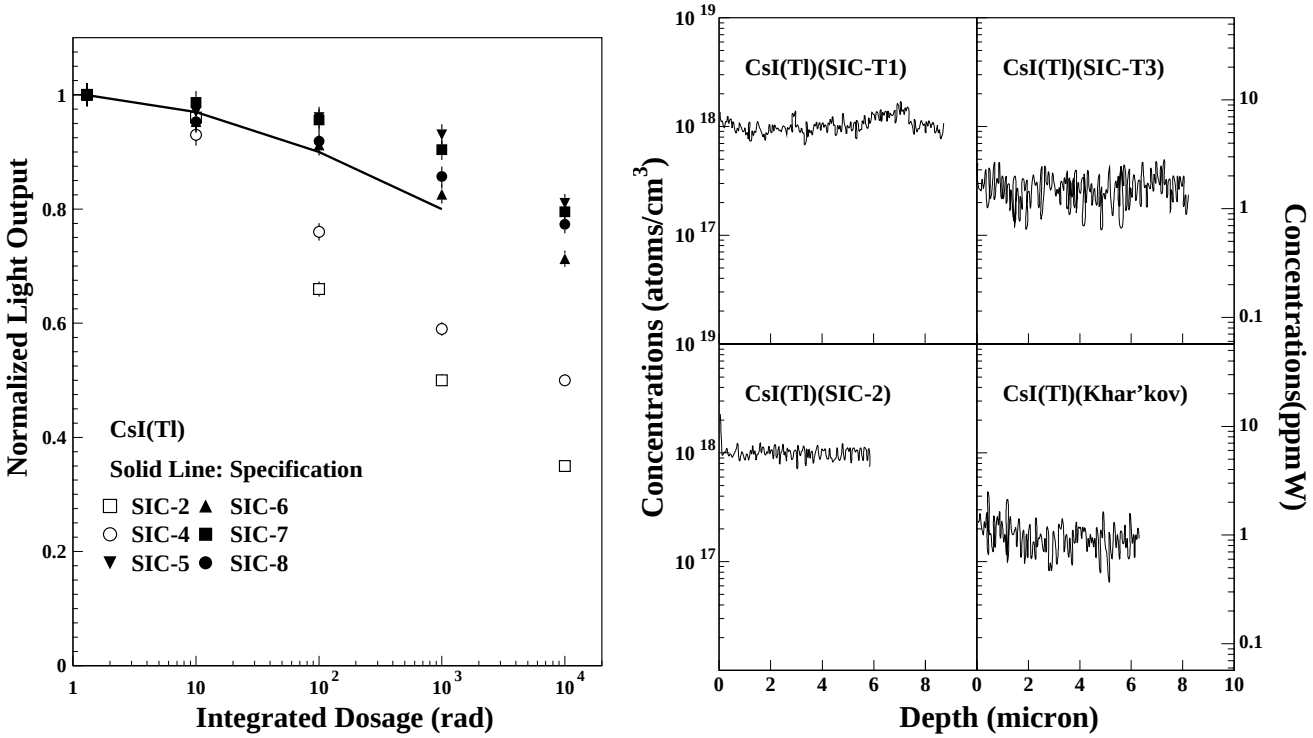

Figure 15. Left: The progress of CsI(Tl) radiation hardness is shown for full size ($\sim$30 cm) CsI(Tl) samples from SIC together with the rad-hard specification of the *BaBar* experiment. Right: The depth profile of oxygen contamination is shown for two rad-soft CsI(Tl) samples (SIC-T1 and SIC-2) and two rad-hard samples (SIC-T3 and Khar'kov).

early samples SIC-2 and 4 did not. This improved radiation hardness of CsI(Tl) crystals was also observed by *BaBar* and BELLE experiments.[19]

The improvement of CsI(Tl) quality was achieved following an understanding that the radiation damage in halide crystals is caused by the oxygen or hydroxyl contamination. The identification of oxygen contamination was achieved by using Secondary Ionization Mass Spectroscopy (SIMS) analysis carried out at Charles Evans & Associates. A Cs ion beam of 6 keV and 50 nA was used to bombard the CsI(Tl) sample. All samples were freshly cleaved prior before being loaded into the UHV chamber. An area of 0.15×0.15 mm^2 on the cleaved surface was analyzed. To further avoid surface contamination, the starting point of the analysis is at about 10 μm deep inside the fresh cleaved surface. Figure 15 (Right) shows the depth profile of the oxygen contamination for two radiation soft samples (SIC-T1 and SIC-2) and two radiation hard samples(SIC-T3 and Khar'kov). Crystals with poor radiation resistance have oxygen contamination of 10^{18} atoms/cm^3 or 5.7 ppmW, which is 5 times higher than the background count (2×10^{17} atoms/cm^3, or 1.4 ppmW). The practical solution at SIC is to use a scavenger to remove oxygen. This leads to the development shown in Figure 15 (Left).

4.2 $PbWO_4$ Development

Figure 16 shows the normalized light output as a function of time under various dose rates for CMS full size (23 cm) $PbWO_4$ samples produced at SIC.[13] Samples produced late 2002 is much more radiation hard than the early samples. This improved radiation hardness of $PbWO_4$ crystals was also confirmed by an evaluation of a batch of mass produced $PbWO_4$ crystals.[20]

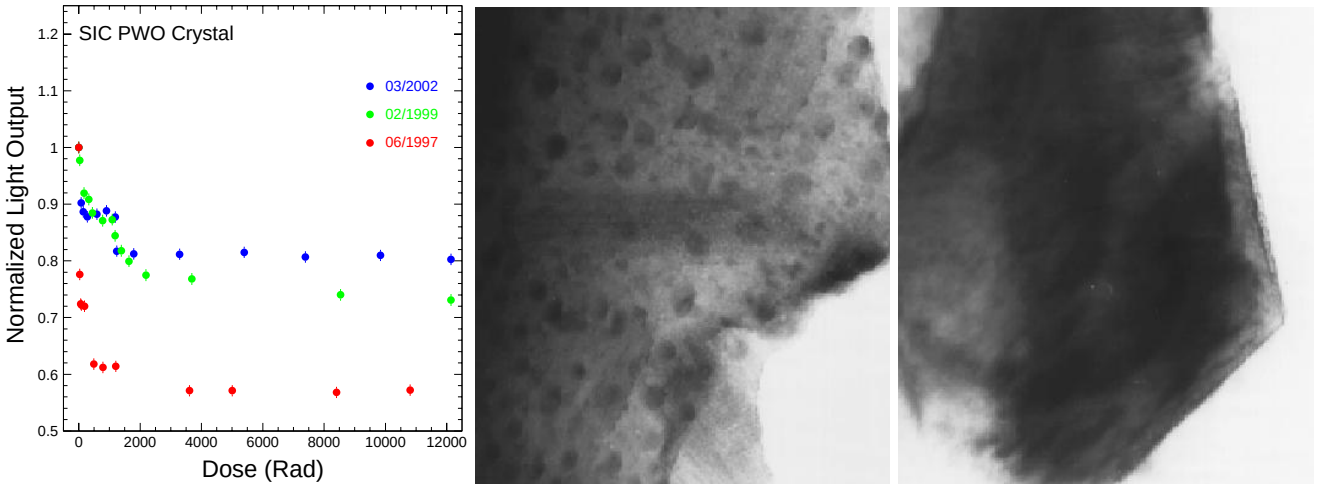

Figure 16. Left: The progress of $PbWO_4$ radiation hardness is shown for full size (23 cm) CMS $PbWO_4$ samples from SIC. TEM pictures of a $PbWO_4$ crystal of poor (Middle) radiation hardness, showing clearly the black spots of ϕ5–10 nm related to oxygen vacancies, as compared to that of a good one (Right)

The improvement of $PbWO_4$ quality was achieved following an understanding that the radiation damage in oxide crystals is caused by the oxygen vacancies. By using Transmission Electron Microscopy (TEM) coupled to Energy Dispersion Spectrometry (EDS), a localized stoichiometry analysis was used to identify oxygen vacancies. A TOPCON-002B Scope was first used at 200 kV and 10 μA. Samples were made to powders of an average grain size of a few μm, and then placed on a sustaining membrane. With a spatial resolution of 2 $\mathring{A}$, the lattice structure of $PbWO_4$ crystals was clearly visible. Figure 16 (Middle) shows a TEM picture taken for a sample with poor radiation hardness. Black spots of a diameter of 5 – 10 nm were clearly seen in the picture. On the other hand, samples with good radiation hardness show stable TEM picture with no black spots, as shown in Figure 16 (Right).

By employing a TEM with EDS system, a localized stoichiometry analysis was carried out at SIC.[21] The system is a JEOL JEM-2010 scope and a Link ISIS EDS. The spatial resolution of this system allows a localized stoichiometry analysis in a region of a diameter of 0.5 nm. An as grown sample was first analyzed, and black spots were observed. Points inside and surrounding the black spots were analyzed as well as points far away from the black spots. The uncertainty of the analysis is about 15%. The resultant atomic fractions (%) at these areas are listed in Table 5.

Table 5. Atomic Fraction (%) of O, W and Pb in $PbWO_4$ Samples Measured by TEM/EDS[21]

As Grown Sample

Element	Black Spot	Peripheral	$Matrix_1$	$Matrix_2$
O	1.5	15.8	60.8	63.2
W	50.8	44.3	19.6	18.4
Pb	47.7	39.9	19.6	18.4

The Same Sample after Oxygen Compensation

Element	$Point_1$	$Point_2$	$Point_3$	$Point_4$
O	59.0	66.4	57.4	66.7
W	21.0	16.5	21.3	16.8
Pb	20.0	17.1	21.3	16.5

A clear deviation from the atomic stoichiometry of O:W:Pb = 66:17:17 was observed in the center of these black spots, pointing to a severe deficit of the oxygen component. In the peripheral area, the oxygen deficit was less, but still significant. There was no oxygen deficit observed in the area far away from the black spots. As a comparison, the same sample after oxygen compensation was re-analyzed. No black spot was found. The result of the analysis is also listed in Table 5. In all randomly selected points no stoichiometry deviation was observed. This analysis thus clearly identified oxygen vacancies in $PbWO_4$ samples of poor radiation hardness.

Various approaches were tried to compensate oxygen vacancies by annealing $PbWO_4$ crystals in an oxygen-rich atmosphere[13] and by doping.[18] Significant improvement of radiation hardness was observed in both cases. The practical solution at SIC is to dope $PbWO_4$ crystals with yttrium. This leads to the development shown in Figure 16 (Left).

5. FUTURE CRYSTAL CALORIMETERS

As discussed in previous sections LSO and LYSO crystals are a new type of crystal scintillators with good light yield 4 and 200 times of BGO and $PbWO_4$ respectively and a fast decay time about 40 ns. The LYSO crystals are also known to be more radiation hard than other crystal scintillators commonly used in high energy and nuclear physics experiment, such as BGO, CsI(Tl) and $PbWO_4$. Mass production capability of LSO/LYSO crystals exists with crystals of size sufficient for crystal calorimeter routinely grown. Assuming the same readout scheme as the CMS $PbWO_4$ calorimeter, the expected energy resolution of an LSO/LYSO crystal based electromagnetic calorimeter would be

$$\sigma_E/E = \mathbf{2}\%/\sqrt{E} \oplus \mathbf{0.5}\% \oplus 0.001/E, \tag{3}$$

which represents a fast calorimeter over large dynamic range with low noise. Such calorimeter would provide great physics discovery potential for high energy physics experiments in the proposed super B factory[22] as well as the proposed International Linear Collider (ILC).[23] Because of its fast scintillation and good radiation hardness LYSO crystals are also proposed for the CMS $PbWO_4$ crystal endcap calorimeter upgrade at SLHC.[24]

Crystals discussed above are used in electromagnetic calorimeter. It is interesting to note that Crystals have recently been proposed to construct a homogeneous calorimeter, including both electromagnetic and hadronic part.[25] This homogeneous hadronic calorimeter concept removes the traditional boundary between ECAL and HCAL, so eliminates the effect of dead materials in the middle of the hadronic shower development. It takes advantage of recently implemented dual readout approach to measure both Cherenkov and scintillation light to achieve good energy resolution for hadronic jets measurement.[26] Because of the unprecedent volume (70 to 100 m^3) foreseen for such calorimeter,[25] the crystal material must be dense (to reduce the volume), UV transparent (to effective collecting the Cherenkov light) and allows a clear discrimination between the Cherenkov and scintillation light.

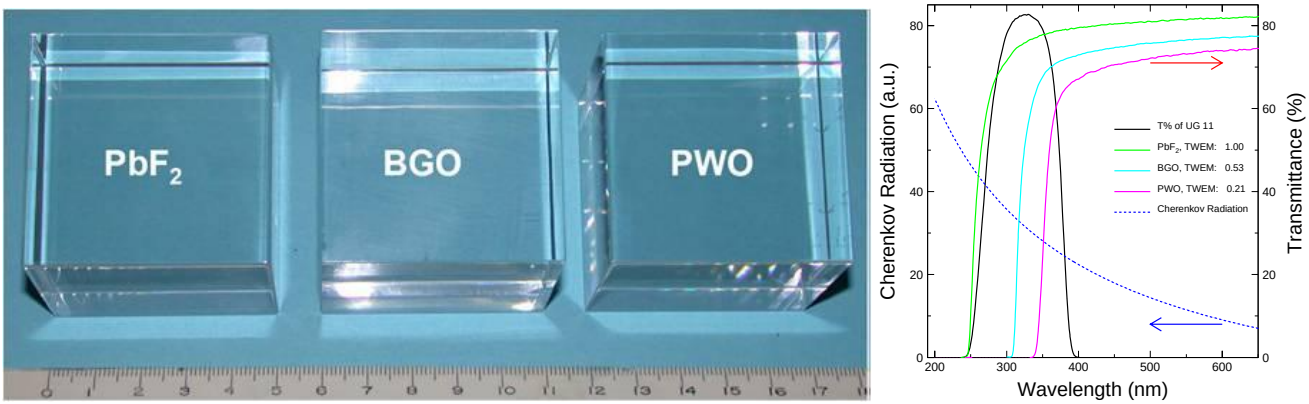

Figure 17. Left: A photo shows three crystal samples of $5\times5\times5\,cm^3$ investigated for the homogeneous hadronic calorimeter concept. Right: The transmittance spectra of PbF_2 (green), BGO (blue), PWO (red) and UG 11 (black) are shown as a function of wavelength. Also shown in this figure are the Cherenkov emission spectrum (dashed blue) and the normalized figure of merit for the Cherenkov light measurement with the UG 11 filter.

Figure 17 (Left) shows samples of three $5 \times 5 \times 5$ cm^3 crystal samples: PbF_2, BGO and PWO. Crystals of this size can be seen as typical building block for a crystal hadronic calorimeter. All material are dense (PbF_2 has of a density of 7.7 g/cm^3) with a nuclear interaction length about 22 cm. Mass production capability exists for all three candidate materials with cost among the lowest for materials of such density. Figure 17 (Right) shows the transmittance spectra of PbF_2 (green), BGO (blue), PWO (red) and a UG 11 filter (black) as a function of wavelength together with the Cherenkov emission spectrum (dashed blue). The UG 11 filter can be used to select the Cherenkov light with small or no scintillation contamination. Also shown in this figure is the normalized figure of merit for the Cherenkov measurement (TWEM) by using the UG 11 filter, which is defined as the transmittance weighted Cherenkov emission spectrum. Their numerical values are 1.0:0.53:0.21, which would be 1.0:0.82:0.75 without using the UG 11 filter. We also note that the values of the cut-off wavelength, at which the transmittance data show 50% of that at 800 nm, are 140 nm, 280 nm, 293 nm, 315 nm, 318 nm, 342 nm, 358 nm, 365 nm and 390 nm for BaF_2, CsI, CeF_3, BGO, CsI(Na), PWO, CsI(Tl), NaI(Tl) and LSO/LYSO respectively. Among all the materials discussed PbF_2 is the second most effective in collecting the Cherenkov light because of its good UV transmission.

Effective discrimination between Cherenkov and scintillation light can be realized by using either spectral difference or light pulse time difference. Recent investigation[27] shows that the use of optical filters, e.g. a UG 11 and a GG400 low pass filters for the Cherenkov and scintillation light respectively, is an effective approach. It, however, was found that there is no difference in the timing and rise time between the Cherenkov and scintillation light pulses, so only the scintillation light pulse width and fall time may be used for this discrimination.[27] A slow scintillator thus may help this discrimination.

Development of cost-effective material is crucial for the homogeneous hadronic calorimeter concept. While BGO is the best material to be used for such calorimeter, R&D is actively pursued by the high energy physics community for additional materials. One approach is to develop PWO crystals with slow scintillation emission. Green (560 nm) and slow emission with a few μsec decay time was observed by selective doping in PWO crystals.[28] Such crystals were reported to have a factor of ten more light than the yttrium doped PWO crystals used in high energy physics experiment. This slow and green scintillation would be desirable for this application.

Another approach is to develop scintillating PbF_2 crystals by selective doping. Observations of fast scintillation in Gd or Eu doped PbF_2 crystals were reported.[29,30] Recent investigation shows that rear earth doping indeed introduces scintillation in PbF_2, but not in the level can be measured by using γ-ray source. Figure 18 shows the excitation, photo-luminescence and x-luminescence spectra for Gd, Sm and Tb doped PbF_2 crystal samples. It is also noted that the scintillation of Sm and Tb doped PbF_2 samples is between 500 to 600 nm, which is desirable for Cherenkov/scintillation discrimination. Investigation is continuing aiming at developing cost-effective materials for this concept.

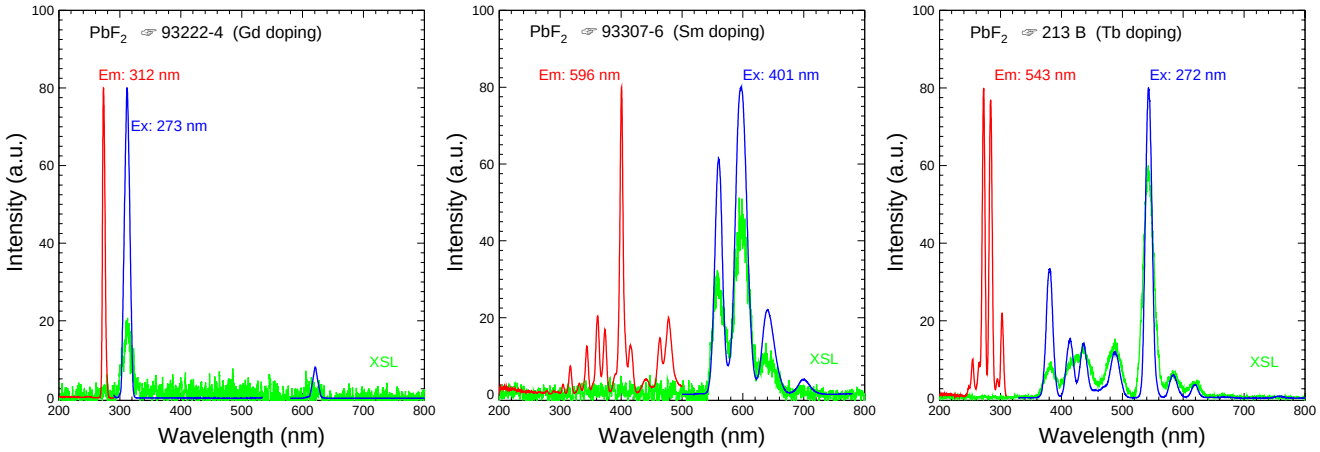

Figure 18. UV excitation (red), photo-luminescence (blue)and x-luminescence (green) spectra are shown as a function of wavelength for Gd (Left), Sm (Middle) and Tb (Right) dopes PbF_2 samples.

6. SUMMARY

Precision crystal electromegnetic calorimeters have been an important part of high energy physics detector. Its energy and position resolutions for electron and photon measurements and photon identification capability has been a key factor in many physics discoveries. In the last two decades it faces a challenge: the radiation damage in scintillation crystals. Progresses have been made in understanding crystal's radiation damage and in developing high quality crystals for high energy physics experiments.

The availability of mass production capability of large size LSO and LYSO crystals provides an opportunity to build a LSO/LYSO crystal electromegnetic calorimeter with unprecedent energy resolution over a large dynamic range down to MeV level. Such calorimeter, if built, would greatly enhance the physics discovery potential for high energy and nuclear physics experiments.

Recent interest in high energy physics community to pursue homogeneous hadronic calorimeter with dual readout opens a new area of crystal calorimetry to achieve good energy resolution for hadronic jets in the next decade. The main challenge for this concept is to develop cost effective heavy crystal scintillators with good UV transmission and excellent Cherenkov/scintillation discrimination.

ACKNOWLEDGMENTS

Work supported by the U.S. Department of Energy Grant No. DE-FG03-92-ER40701 and the U.S. National Science Foundation Award PHY-0612805 and PHY-0516857.

REFERENCES

[1] G. Gratta, H. Newman and R.-Y. Zhu, *Annu. Rev. Nucl. Part. Sci.* **44** 453 (1994).
[2] E. Bloom and C, Peck, *Ann. Rev. Nucl. Part. Sci.* **33** (1983) 143-197.
[3] *The CMS Electromagnetic Calorimeter Project*, CERN/LHCC 97-33 (1997).
[4] R.-Y. Zhu, *Nucl. Instr. and Meth.* **A537** (2005) 344.
[5] U. Chaturvedi *et al.*, *Nucl. Instr. and Meth.* **A461** 376 (2001).
[6] P. Adzic *et al.*, **JINST 2** P04004 (2007).
[7] R.H. Mao, L.Y. Zhang and R.-Y. Zhu, *IEEE Trans. Nucl. Sci.* **NS-55** (2008).
[8] C. Melcher, V.S. Patent 4958080 (1990) and 5025151 (1991).
[9] D.W. Cooke, K.J. McClellan, B.L. Bennett, J.M. Roper, M.T. Whittaker and R.E. Muenchausen, *J. Appl. Phys.* **88** (2000) 7360 and T. Kimble, M Chou and B.H.T. Chai, *2002 IEEE NSS Conference Record*.
[10] E. Loef, P. Dorenbos, E. Eijk, K. Kraemer and H. Guedel, *Nucl. Instr. and Meth.* **A486** (2002) 254.
[11] D.A. Ma and R.-Y. Zhu, *Nucl. Instr. and Meth.* **A333** (1993) 422.
[12] J.M. Chen, R.H. Mao, L.Y. Zhang and R.-Y. Zhu, *IEEE Trans. Nucl. Sci.* **54** (2007) 718.
[13] R.-Y. Zhu, *Nucl. Instr. and Meth.* **A413** (1998) 297–311.
[14] D.A. Ma and R.-Y. Zhu, *Nucl. Instr. and Meth.* **A332** (1993) 113 and **A356** (1995) 309.
[15] J.M. Chen, R.H. Mao, L.Y. Zhang and R.-Y. Zhu, *IEEE Trans. Nucl. Sci.* **54** (2007) 1319.
[16] Z.Y. Wei *et al.*, *Nucl. Instr. and Meth.* **A297** (1990) 163.
[17] R.-Y. Zhu, *Nucl. Instr. and Meth.* **A340** (1994) 442.
[18] X.D. Qu *et al.*, *Nucl. Instr. and Meth.* **A480**, (2002) 470.
[19] T. Hryn'ova, in *Proceedings of the 10th International Conference on Calorimetry in Particle Physics*, World Scientific, Ed. R.-Y. Zhu, (2002) 175.
[20] R.H. Mao, L.Y. Zhang and R.-Y. Zhu, *IEEE Trans. Nucl. Sci.* **NS-51** (2004) 1777.
[21] Z.W. Yin *et al.*, in *Proceedings of SCINT97*, Ed. Zhiwen Yin *et al.*, CAS Press, (1997) 191.
[22] SuperB Conceptual Design Report, **INFN/AE-07/2, SLAC-R-856, LAL 07-15**, March (2007).
[23] R.-Y. Zhu, *An LSO/LYSO Crystal Calorimeter for the ILC*, talk presented in 2005 ILC Workshop, Snowmass. See http://nicadd.niu.edu/cdsagenda//fullAgenda.php?ida=a0561.
[24] R.-Y. Zhu, *Development of LYSO Crystals for CMS at SLHC*, talk presented in CMS ECAL SLHC Workshop, CERN. See http://www.hep.caltech.edu/ zhu/talks/ryz_080415_SLHC.pdf.

[25] A. Para, *Crystal Calorimetry with Dual Readout*, See http://ilcagenda.linearcollider.org/contributionDisplay.py?contribId=15&sessionId=3&confId=2474.
[26] R. Wigmans, *Quartz Fibers and the Prospects for Hadron Calorimetry at 1% Resolution Level*, in *Proceedings of Seventh International Conference on Calorimetry in Particle Physics*, Ed. E. Chen *et al.*, World Scientific (1998) 182, and N. Akchurin *et al.*, *Nucl. Instr. and Meth.* **A537** (2005) 537.
[27] R.Y. Zhu *et al.*, *Crystals for Homogeneous Hadron Calorimeter*, to be presented in *2008 IEEE NSS Conference Record*.
[28] R.H. Mao *et al.*, in *Proceedings of IX International Conference on Calorimetry in Particle Physics*, Ed. B. Aubert *et al.*, Franscati Physics Series Vol. XXI (2000) 709-720.
[29] D. Shen *et al.*, *Jour. Inor. Mater.* **Vol 101** (1995) 11.
[30] C. Woody *et al.*, in *Proceedings of SCINT95*, Delft University Press, Delft, The Netherlands, (1996).